ARTICLE

ZnO/TiO_2 Nanocomposite Synthesized by Sol Gel from Highly Soluble Single Source Molecular Precursor

Hameed Ullah*, Kabeer Ahmad Khan, Wasid Ullah Khan

Department of Chemistry, Hazara University, Mansehra, KPK, Pakistan

(Dated: Received on February 18, 2014; Accepted on August 15, 2014)

Single source molecular precursors (SSPs) provide an opportunity to get control over the microstructure of nanomaterials at atomic level. A SSP was designed and developed for the synthesis of ZnO/TiO_2 nanocomposite by sol gel method. In a typical synthesis process, a bimetallic molecular compound with chemical formula $[Cl_2TiZn(dmae)_4]$ (dmae=dimethylaminoethanol) was synthesized and its chemical composition was determined by elemental analysis. The obtained compound has shown excellent solubility in common organic solvents, a prerequisite for its use in sol gel method as SSP. The SSP obtained was controllably hydrolyzed by adding equimolar amount of water using ethanol as solvent to get ZnO/TiO_2 nanocomposite gel. The resulting gel was precipitated at pH=9 and sintered at 200 °C (T_{200}), 400 °C (T_{400}), and 600 °C (T_{600}). The XRD analyses have shown that the as synthesized (non-sintered, T_{00}) powder was amorphous. However, the crystallinity improved upon sintering, and the XRD analyses revealed that the resulting nanomaterials were composed of mixed oxides *i.e.*, ZnO and TiO_2. The ZnO was in wurtzite (hexagonal) while the TiO_2 was in brookite (orthorhombic) phase. The increase in particle size was further confirmed from BET analysis and SEM micrographs. The IR spectra obtained for the resulting powder have shown the peculiar vibrational bands for Zn−O and Ti−O. Furthermore, the IR spectra revealed that the non-sintered ZnO/TiO_2 nanocomposite had significant number of OH group which was removed upon sintering. The photocatalytic activities of the ZnO/TiO_2 nanocomposites were tested. All the samples have shown good photocatalytic activities. However, the T_{400} has shown higher activity than the T_{00}, T_{200}, and T_{600}. The higher photocatalytic activity of T_{400} than T_{00}, T_{200}, and T_{600} may be due to improved crystallinity which ensures efficient grain boundary interfaces.

Key words: Single source precursor, Sol gel, ZnO/TiO_2, Methyl orange, Photocatalytic activity

I. INTRODUCTION

Nanoscience as well as nanotechnology emerged as a dynamic research field during the last couple of decades. The exponential growth in this interdisciplinary research field is due to the improved characteristics of materials having particle size in the nano (10^{-9} m) domain compared to the bulk materials [1]. The ever-growing use of nanomaterials in different areas pronounces the importance of the nanoscience and subsequently the nanotechnology. By now, nanomaterials have found widespread applications in many devices including photo detectors, surface acoustic, wave devices, UV nanolaser, varistors, solar cells, gas sensors, bio sensor, ceramics, nanogenerator, and field emission devices [2−4]. However, the characteristics, especially the band gap, of semiconductors are influenced mostly by the transition of particle size from bulk into the nanometer lever scale. Among the semiconductors, the conducting oxides (COs) (*e.g.* ZnO, SnO_2, TiO_2 *etc.*) have been researched and investigated the most for their possible use as photocatalysts [5, 6]. The organic dyes are notorious environmental pollutants which could be degraded under sunlight using the COs as photocatalysts [5, 6]. Among these different COs photocatalysts, TiO_2 and ZnO are important nanomaterials owning fascinating physico-chemical characteristics.

TiO_2 is a versatile photocatalyst and has been used for the photo-degradation of organic environmental pollutants. The attractiveness of TiO_2 as a photocatalyst is due to its many positives properties, including higher photocatalytic activity, absence of toxicity, relatively low cost, and excellent chemical stability under various conditions [7, 8]. Among these many positive characteristics of TiO_2, the high photocatalytic activity as a photocatalyst is fascinating and attractive for the researchers and market promoters. The high photo-

*Author to whom correspondence should be addressed. E-mail: hameedwazir@yahoo.co.uk, FAX: +92-997-530046

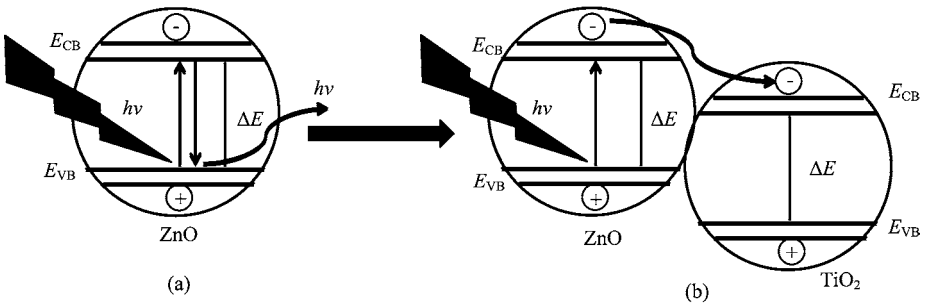

FIG. 1 Electron-hole pair recombination in single oxide (a) and separationin coupled oxides (b).

catalytic activity of TiO_2 corresponds to its wide direct band gap and suppressed photo-generated electron-hole pair. The long life of the photo-generated electron-hole pair is highly desirable because the photo-generated electron-hole pair is responsible for the initiation of a number of reactions which eventually decompose the hazardous organic molecules and thus minimize the environmental pollutants [9, 10]. Very recent reports show that the single crystalline TiO_2 in brookite phase has excellent properties surpassing the other phases of TiO_2 [11−13].

ZnO, besides TiO_2, is another interesting photocatalyst which attracts a tremendous deal of research attention, contemporarily. ZnO like TiO_2 has many unique properties, electrical and optical, which pronounce its role as a COs semiconductor. The fascinating electrical and optical properties presented ZnO as a potential candidate for many applications in diverse areas. ZnO by now has been used in conducting films, wave guides, UV lasers, solar cells, photocatalysis, and varistors [14]. Among the various applications of ZnO, it has been regarded as a highly active photocatalyst in environmental pollutants degradation because ZnO has a similar photodegradation mechanism as TiO_2 [15, 16]. Besides the similarity in photodegradation mechanism, ZnO and TiO_2 have comparable band gap energy [17]. Although, ZnO and TiO_2 have very good reputation as photocatalysts, but the two have many deficiencies as photocatalysts in their individual capacities. One of the main problems of the individual ZnO (TiO_2 as well) is the fast electron-hole pair recombination which adversely affects the efficiency and photo enhanced photocatalytic activity of the materials [18]. Bandara *et al.* showed that the fast electron-hole pair recombination in ZnO could be suppressed by coupling with SnO_2 [19]. They proposed that the electrons generated in the ZnO crystallite passed into the SnO_2 crystallite through the grain boundary interface and thus moved away from the hole in the ZnO crystallite (Fig.1). The success of electron transfer from one oxide crystallite into the other depends upon the efficiency of the grain boundary interface.

The efficient grain boundary interface could be achieved successfully by restricting the particle size in nanometer level scale. The nanoparticles have large surface area and thus provide a large number of active sites for interaction among the particles of different oxides. To achieve the ZnO/TiO_2 nanocomposite having particle size, strictly, in the nano domain, many preparatory methods have been used for the synthesis of ZnO/TiO_2 nanomaterials. The different processes so far applied for the preparation of ZnO/TiO_2 include solid state reaction [9, 10], hydrothermal reaction [14, 15], magneton sputtering [16, 17] *etc.* However, these methods have one common problem of using multiple sources precursors (mostly inorganic salts) which hinder the control over the microstructure (particle size, shape, crystal structure *etc.*), on one hand. On the other hand, these multiple sources precursors are responsible for high degree contamination of the resulting products. Mathur *et al.* proved that the precursor role was vital in controlling the microstructure of the nanomaterials [20]. Therefore, it is highly desirable that the constituents of the resulting nanomaterial must be accumulated in a single chemical molecule called as single source precursor (SSP). SSPs have the advantages of lower decomposition temperatures [20]. Besides, the resulting nanomaterials obtained from SSPs have enhanced characteristics such as higher homogeneity in the size and shape of the particles, and higher purity of the ultimate product which is observed previously as well [21].

Here we report the synthesis of heterometal zinc titanium SSP and its application in sol gel process for preparation of ZnO/TiO_2 nanocomposite. The resulting nanomaterial showed fascinating photocatalytic activity for the degradation of methyl orange (MO) taken as a test case.

II. EXPERIMENTS

A. Materials and methods

All the chemicals were purchased from commercial suppliers and used as received without further purifications. Titanium tetrachloride ($TiCl_4$), *N*,*N*-dimethyleamino-2-ethanol (dmaeH), NaOH, and zinc chloride ($ZnCl_2$) were from the Sigma-Aldrich company

DOI:10.1063/1674-0068/27/05/548-554

while ethanol was from Acros-organics. Doubly distilled water was produced in our own laboratory. The elemental composition of the precursor was determined by CHN analyzer (LECO CHN 900). The powder XRD patterns of the samples were recorded on X-Ray diffractometer (X Pert PRO) with Cu Kα radiations. IR spectra of the ZnO/TiO_2 nanocomposite powder were recorded by IR spectrophotometer (Nicolet 6700). Scanning electron microscope (SEM) of the Jeol Company (JSM-6490A) was also used. The surface areas of the ZnO/TiO_2 nanocomposites were determined by Brunauer-Emmett-Teller (BET) method using gaseous nitrogen as adsorbate in the nitrogen adsorption instrument of Micromeritics. The samples were degassed at elevated temperature before the surface area(s) measurement by the BET instrument. The photocatalytic study was followed by UV-visible spectrophotometer of the Schimadzu company (Pharma Spec UV-1700) using quartz cuvettes.

B. Synthesis of $[Cl_2TiZn(dmae)_4]$ SSP

The SSP (molecular) was synthesized by dissolving 2.00 g (14.67 mmol) of $ZnCl_2$ in 15 mL absolute ethanol at room temperature. An equimolar (2.783 g, 14.67 mmol) of $TiCl_4$ was dissolved in absolute ethanol under cooling (ice bath was used) and slowly added into the $ZnCl_2$ solution from pressure equalizing dropping funnel. After stirring this solution mixture for 1 h, 5.231 g (58.69 mmol) of dmaeH dissolved in absolute ethanol was added drop by drop from dropping funnel. As soon as the addition of dmaeH started, white fumes were observed in the reaction flask. The dense fumes were collected and condensed by the addition of doubly distilled water and later titrated with NaOH. The fumes were confirmed as HCl, after titration with NaOH, NaCl was obtained. After washing and purification, 7.03 g (89.3%) of the SSP was obtained as thick yellowish transparent liquid.

C. Preparation of ZnO/TiO_2 photocatalyst

2.5 g of the precursors $[Cl_2TiZn(dmae)_4]$ was dissolved in 50 mL of ethanol and was stirred to get homogenous solution. A stoichiometric amount of water was added drop-wise into the precursor solution. After stirring for 10 min, the gel formation started. The solution mixture was stirred for another 4 h to complete the gelation process. The pH of the solution was raised to 9 by adding NaOH solution. The white precipitate was filtered off and dried at 120 °C in laboratory oven over night. The dried ZnO/TiO_2 nanocomposite was sintered in furnace at 200, 400, and 600 °C for 4 h. The resulting powders were stored in clean and dry ampules, and named as T_{00} (unsintered), T_{200} (sintered at 200 °C), T_{400} (sintered at 400 °C), and T_{600} (sintered at 600 °C).

D. Degradation of MO using ZnO/TiO_2 Photocatalyst

The photoinduced catalytic degradation of MO as test case was carried out by preparing MO solution in doubly distilled water. The photocatalytic reactor was an assemblage of different devices, including a pyrax bottle holding the solution and a high pressure Hg lamp (300 W) with a maximum emission at 365 nm. The lamp was positioned paralle to the pyrax bottle and the reaction temperature was maintained at 25±2 °C. The pyrax reaction flask was covered with black paper from all the sides except a small window at the side of the illuminating lamp. 0.25 g of ZnO/TiO_2 photocatalyst (T_{00}) was added into the 250 mL of MO solution and stirred for 30 min to establish the adsorption/desorption equilibrium. 10 mL of the MO orange solution was taken before the illumination of lamp and was filtered. The filterate was analyzed by UV-visible spectrophotomtere. After 30 min of lamp illumination, a 10 mL of the solution was taken, filtered and the filterate was analyzed by UV-visible spectrophotometere. The same procedure was repeated after 60, 90, and 120 min.

Following the above steps the photocatalytic activities of the ZnO/TiO_2 nanocomposites, T_{200}, T_{400}, and T_{600} were determined.

III. RESULTS AND DISCUSSION

A. Molecular SSP

The molecular SSP was obtained as a thick yellowish transparent liquid. The compound was subjected to crystallization by different techniques. However, all the efforts failed to get crystals (or even solid powder) of the compound. The white fumes produced during the reaction were trapped into a flask and condensed by adding cold water. The resulting water dissolved fumes were titrated against NaOH and confirmed that the fumes were HCl produced during the reaction. Based upon the analysis, the following reaction is proposed for the synthesis of the molecular SSP (reaction (1)). It is pertinent to mention here that the reactions in which 5 and 6 equivalent of dmaeH were used, did not give a single phased resulting product and were ignored as molecular SSP. However, the investigations are under progress for such type of compounds and their structural characterization will be reported elsewhere.

$$TiCl_4+ZnCl_2+4dmaeH \xrightarrow{EtOH} Cl_2TiZn(dmae)_4+4HCl \quad (1)$$

The elemental composition of the molecular SSP was determined by CHN analyzer and the chlorine

DOI:10.1063/1674-0068/27/05/548-554

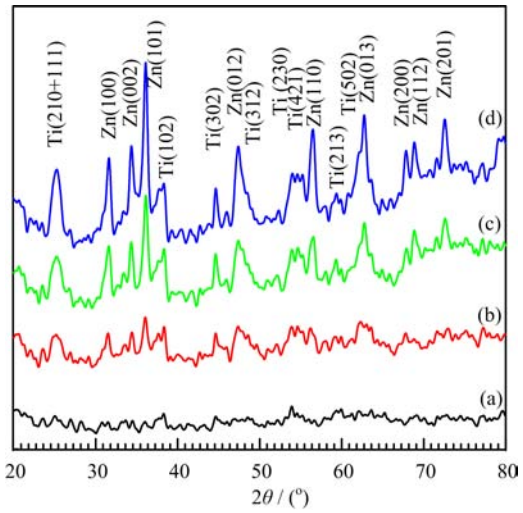

FIG. 2 XRD patterns of ZnO/TiO_2 nanocomposite synthesized by sol gel method from molecular SSP. (a) T_{00}, (b) T_{200}, (c) T_{400}, and (d) T_{600}.

TABLE I Elemental composition of molecular SSP.

Method	Composition/%			
	C	H	N	Cl
Calc.	35.81	7.51	10.44	13.21
Expt.	34.94	7.37	10.61	13.05

contents were determined argentometrically (Table I). Based upon the elemental analysis the chemical formula, $Cl_2TiZn(dmae)_4$ was suggested for the molecular SSP. The compound showed excellent solubility in the common organic solvents (methanol, ethanol, toluene, chloroform, and benzene) which was required for the synthesis of ZnO/TiO_2 by sol gel method.

B. ZnO/TiO_2 nanocomposite

The ZnO/TiO_2 nanocomposite was synthesized by dissolving the required amount of molecular SSP in ethanol. The resulting white powder was precipitaed at pH=9 using NaOH as pH adusting reagent. The white powder was subjected to sintering in muffle furnace at temperature 200, 400, and 600 °C. The color of the powder remains the same upon heating in furnace. All the samples (T_{00}, T_{200}, T_{400}, and T_{600}) were characterized by powder XRD technique. Figure 2 shows the XRD patterns of the ZnO/TiO_2 nanocomposite samples T_{00}, T_{200}, T_{400}, and T_{600}. XRD pattern of T_{00} does not give any significant peak in the 2θ region of 20°−80°. This indicates that the as synthesized ZnO/TiO_2 is amorphous. However, the XRD patterns of T_{200}, T_{400}, and T_{600} give reasonable peaks indicating the transition of ZnO/TiO_2 nanocomposite from amorphous to crystalline phase upon heating. The peaks in the XRD pattern of T_{200} are broad, unclear and less intense. It indicates that the ZnO/TiO_2 nanocomposite has crystallized at 200 °C. However, the crystallite sizes for ZnO and TiO_2 were very small in the range of 1−2 nm, which have been calculated from the broadening of the peaks using Scherrer equation:

$$D = \frac{0.94\lambda}{\beta_{1/2}\cos\theta} \tag{2}$$

The XRD pattern of T_{400} gives more intense and clear peaks compared to that of T_{200}. This means that the crystallite size improved upon heating upto 400 °C. the crystallite size calculated from Scherrer equation is 8−10 and 2−5 nm for ZnO and TiO_2, respectively. Well defined peaks are observed in the XRD pattern of T_{600}. The crystallite size of ZnO and TiO_2 are in the ranges of 5−8 and 15−20 nm, respectively. The improved crystallinity upon heating the ZnO/TiO_2 nanocomposite upto 600 °C provides the opportunity to match the XRD pattern of ZnO/TiO_2 nanocomposite with that of the standard. The peaks appearing at 2θ=31.61°, 34.36°, 36.09°, 47.37°, 56.50°, 67.87°, 68.84°, and 72.54° correspond to the ZnO reference pattern (PDF: 96-230-114). While the peaks at 25.32°, 30.84°, 38.27°, 44.19°, 53.92°, 55.17°, 59.34°, and 62.05° correspond to the XRD pattern of TiO_2 (PDF: 6-900-4140). The peak at 2θ=25.32° is quite very broad which indicates the overlap of TiO_2 lattice planes (210) and (111). The ZnO peak at 31.61° overlaps with the TiO_2 peak of (211) plane which is shown as shoulder upon the ZnO(100) plane peak. The XRD characterization confirms the composition of the samples as ZnO/TiO_2, and also confirms the phases of constituents *i.e.*, ZnO and TiO_2 as hexagonal (wurtzite) and orthorhombic (brookite), respectively. It is also confirmed that the crystallity has improved significantly upon heating the samples in furnace.

The increase in crystallite size as function of sintering temperature was also confirmed by BET and SEM techniques. The surface areas of the ZnO/TiO_2 nanocomposites were 14.30, 9.63, 6.90, and 4.13 m^2/g for samples T_{00}, T_{200}, T_{400}, and T_{600}, respectively. It is evident that the surface area decreases as the sintering temperature increases. It is also previously observed that with increasing sintering temperature, though the crystallinity improves, the surface area decreases [22]. The decrease in surface area is due to the increase in crystallite and particle size of the ZnO/TiO_2 nanocomposites.

Figure 3 gives the SEM images of the samples T_{00}, T_{200}, T_{400}, and T_{600}. The SEM image of sample T_{00} gives particles of nearly uniform size in the nano domain (Fig.3(a)). The particles vary in their shapes with some agglomeration. It is seen in the Fig.3(b) that the particles are nearly spherical, and interfused after sintering the sample at 200 °C. However, the increase in particle size with sintering temperature is more evident from

DOI:10.1063/1674-0068/27/05/548-554

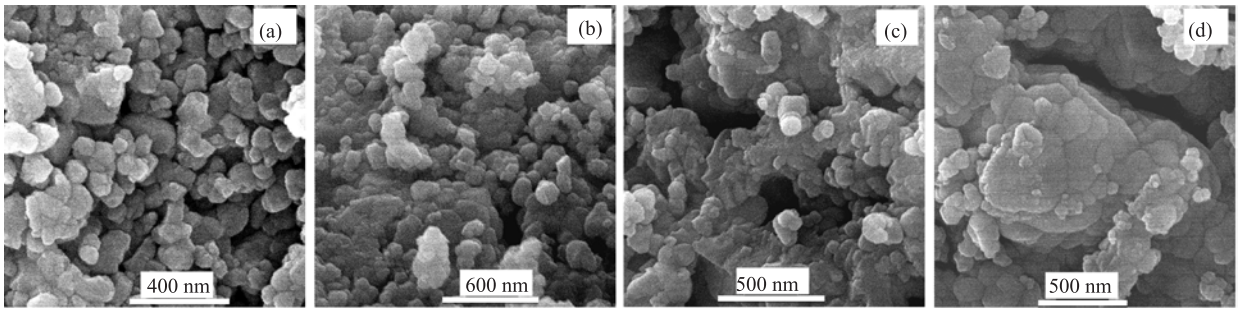

FIG. 3 SEM images of ZnO/TiO_2 nanocomposites. (a) T_{00}, (b) T_{200}, (c) T_{400}, and (d) T_{600}.

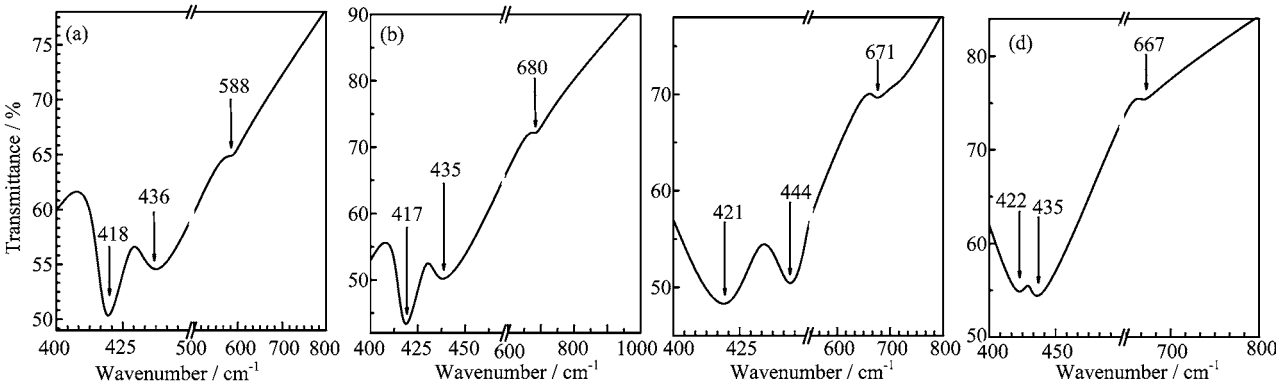

FIG. 4 IR spectra of ZnO/TiO_2 nanocomposite; (a) T_{00}, (b) T_{200}, (c) T_{400}, and (d) T_{600}.

the SEM images of the samples T_{400} and T_{600} given in Fig.3 (c) and (d), respectively.

All the samples were characterized by IR spectroscopy as well (Table II and Fig.4). The IR spectrum of T_{00} gives a broad peak at 3346 cm^{-1} corresponding to the O−H stretching vibration [23]. Peaks observed in the range of 1700−1500 cm^{-1} are due to the bending vibrations of adsorbed H_2O and OH group [22]. The peaks in the region of 700−400 cm^{-1} are assigned to the Zn−O and Ti−O vibrations [24]. The peaks at 436 and 418 cm^{-1} in the IR spectrum of T_{00} are due to the Zn−O vibration [25]. While the peak at 588 cm^{-1} could be due to the Ti−O vibration [23].

The IR spectrum of T_{200} is different from that of T_{00} in the region of 4000−1000 cm^{-1}. The broad peak around 3400 cm^{-1}, and also, the peaks in the range of 1700−1500 cm^{-1} are absent. This indicates that upon heating the adsorbed H_2O, and the attached OH groups are removed. However, in the 700−400 cm^{-1} region, the IR spectrum of T_{200} is comparable to that of T_{00} with some exceptions. The Zn−O vibration bands appear at 435 and 417 cm^{-1}. However, the band for Ti−O vibration shifts to around 680 cm^{-1}. This is not an un-precedented move as the IR spectra are dictated by the size and shape of the particle [26]. The IR spectrum of T_{400} is identical to that of T_{200} in the region of 4000−1000 cm^{-1} where there are not any significant peaks. An insignificant peaks could be seen, as well, which are due to the adsorption of small amount of H_2O during the sample processing for IR analysis. The Zn−O peculiar peaks appear at 444 and 421 cm^{-1} while the peaks for Ti−O could be seen around 671 and 503 cm^{-1} which corresponds to that of brookite TiO_2 [27]. The IR spectrum of T_{600} gives peak at 435 and 422 cm^{-1} for Zn−O corresponding to the spectra of T_{00}, T_{200}, and T_{400} [25]. A Ti−O peculiar peak appears at 667 cm^{-1} in the IR spectrum of T_{600}.

TABLE II Values of the bands of ZnO/TiO_2 IR spectra.

Sample	IR band/cm^{-1}		
	O−H	Zn−O	Ti−O
T_{00}	3346	436, 418	588
T_{200}		435, 417	680
T_{400}		444, 421	671
T_{600}		435, 422	667

C. Photocatalytic activity of ZnO/TiO_2 nanocomposite

The ZnO/TiO_2 nancomposites were used a photocatalyst for the degradation of MO dye, taken as test case (Fig.5). The dye degradation is the result of series of chemical reactions [28]. All the four samples *i.e.*, T_{00}, T_{200}, T_{400}, and T_{600} showed excellent photocatalytic

DOI:10.1063/1674-0068/27/05/548-554

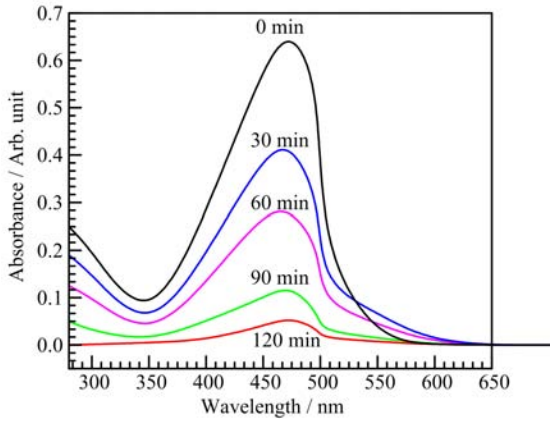

FIG. 5 Photocatalytic degradation of MO dye using T_{400} sample.

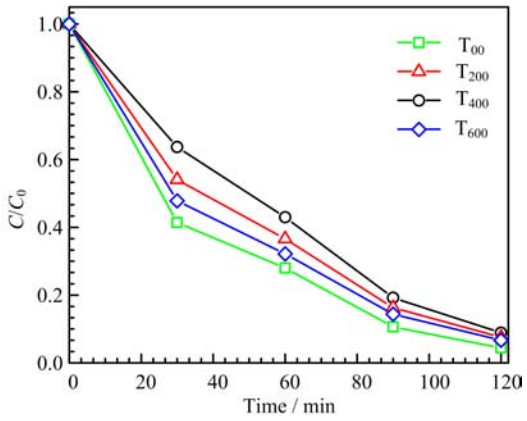

FIG. 6 MO degradation using photocatalysts ZnO/TiO_2.

activity. More than 70% of the MO was degraded after 120 min of exposure to the irradiating lamp. However, it is pertinent to mention here that the photocatalytic activity of T_{400} sample was more than those of T_{00}, T_{200}, and T_{600} (Fig.6). This indicates that the photocatalytic activity is enhanced with sintering the sample upto 400 °C and then decreases.

The sintering temperature effect upon the photocatalytic activity of nanomaterials has been reported previously as well. Xia *et al.* observed that the photocatalytic activity of CuO−SnO_2 was enhanced upon sintering upto 500 °C and then decreased [29]. As the sintering temperature increased the crystallinity improved, allowing better and enhanced grain boundary interfaces. Subsequently, the electron transfer from one particle to the other became more efficient. The effective electron transfer hindered the electron-hole pair recombination and the dye degradation rate increased due to the availability of dye radicals for further reactions. However, at sintering temperature of 600 °C, the particle (crystallite) size increases sufficiently, and consequently, the surface area of the photocatalyst decreased, and thus the photocatalytic activity of ZnO/TiO_2 also decreased [29].

IV. CONCLUSION

A new molecular SSP was designed and developed for the synthesis of ZnO/TiO_2 nanocomposite by sol gel method. The accumulation of all the necessary elements of ZnO/TiO_2 nanocomposite in a single molecule, the controlled hydrolysis of the SSP, and high solubilty of the molecualr SSP in organic solvent (to give homogenoues solution) allowed better control over the microstructure of ZnO/TiO_2 nanocomposite. Also, owing to the above mentioned advantageous factors of molecualr SSP, the constituents of the ZnO/TiO_2 nanocomposite are obtained in single crystalline phase (wurtzite ZnO, and brookite TiO_2) which is normally very difficult, especially in case of TiO_2, by using conventional metal salts as precursors. The single crystalline phases of ZnO and TiO_2 were confirmed by powder XRD analysis. The resulting ZnO/TiO_2 nanocomposites have crystallite size well below 20 nm and show excellent photocatalytic activities. The sintering temperature effect upon the photocatalytic activity of ZnO/TiO_2 nanocomposite has been studied and it is confirmed that the best results are obtained with ZnO/TiO_2 nanocomposite sintered at 400 °C. The lower photocatalytic activity of the as synthesized and sintered at 200 °C ZnO/TiO_2 nanocomposites are due to the poor grain boundary interfaces. While the lower photocatalytic activity of the ZnO/TiO_2 nanocomposite sintered at 600 °C could correspond to the increased particle (crystallite), and eventaully the decreased surface area. The increase in particle size as a function of sintering temperature is evident from the XRD, BET, and SEM results.

[1] A. Henglein, Chem. Rev. **89**, 1861 (1989).
[2] W. Water and S. Y. Chu, Mater. Lett. **55**, 67 (2012).
[3] Y. Huang. M. Lius, S. Jiang, Y. Zeng, C. Li, S. Liu, and D. Zhou, Microelectron. Eng. **66**, 760 (2003).
[4] H. Satu, T. Mianini, Y. Tamura, S. Takate, T. Moouri, and N. Ogauua, Thin Solid Film **246**, 86 (1994).
[5] N. M. Dimitrijevic, Z. V. Saponjic, B. M. Rabatic, and T. Rajh, J. Am. Chem. Soc. **127**, 1344 (2005).
[6] B. Mrabatlu, N. M. Dimitrijevice, and R. E. Cook, Adv. Mater. **18**, 1033 (2006).
[7] S. J. Liao, D. G. Huang, D. H. Yi, Y. L. Su, and G. Q. Yuan, J. Photochem. Photobiol. **168**, 7 (2004).
[8] R. Compardi, E. Fanizza, M. L. Cum, P. D. Corri, G. Mascolo, and A. Agostiano, Appl. Catal. B **60**, 1 (2005).
[9] M. Muruganandhem and M. Swaminathan, Energy Matter. Sol. Cell **81**, 439 (2004).
[10] L. Q. Jing, B. F. Xiu, F. L. Yuan, B. O. Wang, K. Y. Shi, and W. M. Cai, Appl. Catal. **275**, 49 (2004).

DOI:10.1063/1674-0068/27/05/548-554

[11] H. Lin, L. Li, M. Zhao, X. Huang, X. Chen, G. Li, and R. Yu, J. Am. Chem. Soc. **134**, 8328 (2012).
[12] M. Zhao, L. Li, H. Lin, L. Yang, and G. Li, Chem. Commun. **49**, 7046 (2013).
[13] M. Guo, L. Li, H. Lin, Y. Zuo, X. Huang, and G. Li, Chem. Commun. **49**, 11752 (2013).
[14] M. H. Cho and G. H. Lec, Thin Solid Film **516**, 5877 (2008).
[15] C. Q. Ge, C. S. Xie, M. L. Hu, X. H. Gui, Z. K. Bai, and D. W. Zeng, Mat. Sci. Eng. B **141**, 43 (2007).
[16] Y. Zhou, W. B. Wu, Ghu, H. T. Wu, and S. G. Cui, Mat. Res. Bull. **43**, 2113 (2008).
[17] L. E. Greene, M. Law, B. D. Yuhas, and P. Yang, J. Phys. Chem. C **111**, 18451 (2007).
[18] M. A. Aramendia, V. Borau, J. C. Colmenares, A. Marinas, J. M. Marinas, J. A. Navio, and F. J. Urbano, Appl. Catal. B **80**, 88 (2008).
[19] J. Bandara, K. Tennakone, and P. P. B. Jayatilaka, Chemosphere **49**, 439 (2002).
[20] S. Mathur, M. Veith, T. Ruegamer, E. Hemmer, and H. Shen, Chem. Mater. **16**, 1304 (2004).
[21] M. Veith, S. Faberr. R. Hempelmann, S. Janssen, J. Prewoh, and H. Eckerlebe, J. Mater. Sci. **31**, (1996) 2009.
[22] J. G. Yu, X. J. Zhao, and Q. N. Zhao, Mater. Chem. Phys. **69**, 25 (2001).
[23] S. S. Mali, C. A. Betty, P. N. Bhosale, and P. S. Patil, ECS J. Solid State Sci. Technol. **1**, 15 (2012).
[24] A. Stoyanova, H. Hitkova, A. Bachvarova-Nedelcheva, R. Iordanova, N. Ivanova, and M. Sredkova, J. Chem. Technol. Metall. **48**, 154 (2013).
[25] R. Gegova, Y. Dimitriev, A. Bachvarova-Nedelcheva, R. Iordanova, A. Loukanov, and Tz. Iliev, J. Chem. Technol. Metall. **48**, 147 (2013).
[26] J. L. Rendon and C. J. Serna, Clay Minerals **16**, 375 (1981).
[27] W. Hu, L. Li, G. Li, C. Tang and L. Sun, Crys. Growth Des. **9**, 3676 (2009).
[28] M. A. Habib, M. T. Shahadat, N. M. Bahadur, I. M. I. Ismail, and A. J. Mahmood, Int. Nano Lett. **3**, 5 (2013).
[29] H. L. Xia, H. S. Zhuang, T. Zhang, and D. C. Xiao, J. Environ. Sci. **19**, 1141 (2007).

DOI:10.1063/1674-0068/27/05/548-554